Research Article

Decellularized optic nerve functional scaffold transplant facilitates directional axon regeneration and remyelination in the injured white matter of the rat spinal cord

https://doi.org/10.4103/1673-5374.310696
Date of submission: September 17, 2020
Date of decision: November 12, 2020
Date of acceptance: January 21, 2021
Date of web publication: March 25, 2021

Yu-Rong Bai[1, 2, #], Bi-Qin Lai[1, 2, 3, 4, 5, *, #], Wei-Tao Han[1, 2], Jia-Hui Sun[1, 2], Ge Li[1, 2], Ying Ding[1, 2, 4, 5], Xiang Zeng[1, 2, 4, 5], Yuan-Huan Ma[1, 2, 4, 5], Yuan-Shan Zeng[1, 2, 3, 4, 5, *]

Graphical Abstract *Decellularized optic nerve functional scaffold containing neurotrophin-3-overexpressing Schwann cells facilitates directional regeneration and remyelination of axons during the repair of white matter injury*

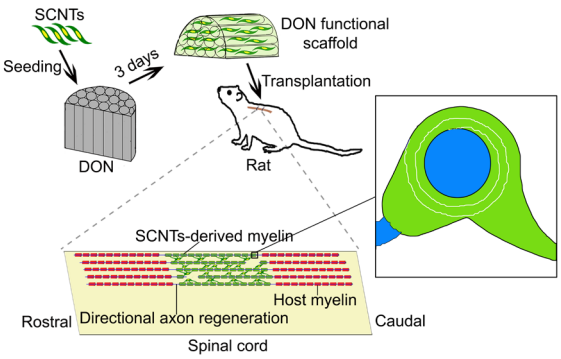

Abstract

Axon regeneration and remyelination of the damaged region is the most common repair strategy for spinal cord injury. However, achieving good outcome remains difficult. Our previous study showed that porcine decellularized optic nerve better mimics the extracellular matrix of the embryonic porcine optic nerve and promotes the directional growth of dorsal root ganglion neurites. However, it has not been reported whether this material promotes axonal regeneration *in vivo*. In the present study, a porcine decellularized optic nerve was seeded with neurotrophin-3-overexpressing Schwann cells. This functional scaffold promoted the directional growth and remyelination of regenerating axons. *In vitro*, the porcine decellularized optic nerve contained many straight, longitudinal channels with a uniform distribution, and microscopic pores were present in the channel wall. The spatial micro topological structure and extracellular matrix were conducive to the adhesion, survival and migration of neural stem cells. The scaffold promoted the directional growth of dorsal root ganglion neurites, and showed strong potential for myelin regeneration. Furthermore, we transplanted the porcine decellularized optic nerve containing neurotrophin-3-overexpressing Schwann cells in a rat model of T10 spinal cord defect *in vivo*. Four weeks later, the regenerating axons grew straight, the myelin sheath in the injured/transplanted area recovered its structure, and simultaneously, the number of inflammatory cells and the expression of chondroitin sulfate proteoglycans were reduced. Together, these findings suggest that porcine decellularized optic nerve loaded with Schwann cells overexpressing neurotrophin-3 promotes the directional growth of regenerating spinal cord axons as well as myelin regeneration. All procedures involving animals were conducted in accordance with the ethical standards of the Institutional Animal Care and Use Committee of Sun Yat-sen University (approval No. SYSU-IACUC-2019-B034) on February 28, 2019.

Key Words: axonal regeneration; decellularized optic nerve; directional regeneration; functional scaffold; microenvironment; neurotrophin-3; optic nerve; remyelination; Schwann cells; tissue engineering; white matter injury

Chinese Library Classification No. R456; R744; R318.08

[1]Key Laboratory for Stem Cells and Tissue Engineering, Ministry of Education, Sun Yat-sen University, Guangzhou, Guangdong Province, China; [2]Department of Histology and Embryology, Zhongshan School of Medicine, Sun Yat-sen University, Guangzhou, Guangdong Province, China; [3]Co-innovation Center of Neuroregeneration, Nantong University, Nantong, Jiangsu Province, China; [4]Institute of Spinal Cord Injury, Sun Yat-sen University, Guangzhou, Guangdong Province, China; [5]Guangdong Provincial Key Laboratory of Brain Function and Disease, Zhongshan School of Medicine, Sun Yat-sen University, Guangzhou, Guangdong Province, China
***Correspondence to:** Bi-Qin Lai, MD, laibiqin@126.com; Yuan-Shan Zeng, MD, zengysh@mail.sysu.edu.cn.
https://orcid.org/0000-0003-1978-3466 (Bi-Qin Lai); 0000-0003-3804-5792 (Yuan-Shan Zeng)
#Both authors contributed equally to this work.

Funding: *This work was supported by grants from the National Key R&D Program of China, No. 2017YFA0104704 (to BQL); the Young Elite Scientist Sponsorship Program (YESS) by China Association for Science and Technology (CAST), No. 2018QNRC001 (to BQL); the Fundamental Research Funds for the Central Universities, China, No. 18ykpy38 (to BQL); and the National Natural Science Foundation of China, Nos. 81971157 (to BQL), 81891003 (to YSZ).*
How to cite this article: *Bai YR, Lai BQ, Han WT, Sun JH, Li G, Ding Y, Zeng X, Ma YH, Zeng YS (2021) Decellularized optic nerve functional scaffold transplant facilitates directional axon regeneration and remyelination in the injured white matter of the rat spinal cord. Neural Regen Res 16(11):2276-2283.*

Introduction

Spinal cord injury (SCI) can lead to disruption of descending and ascending axons, myelin degeneration, and a hostile microenvironment, which can result in severe sensorimotor dysfunction. This can be addressed by mitigating the detrimental microenvironment and facilitating the regeneration and remyelination of axons (Biernaskie et al., 2007; Plemel et al., 2014; Li et al., 2016). A tissue-engineering strategy including scaffolds with neurotrophic factors and seeded cells has emerged as a promising therapy for SCI.

David and Aguayo (1981) found that transplanting a segment of peripheral nerve into an SCI lesion promotes the regeneration of neuronal axons. The study showed that even axons of host neurons in central nervous tissue can regenerate into the lesion, as long as the microenvironment of the injury/graft area is suitable. A more recent study showed that transplanted Schwann cells (SCs) can not only wrap axons and form the myelin sheath but also secrete a variety of neurotrophic factors to promote the survival and axonal regeneration of host neurons (Sparling et al., 2015). In previous study, we showed that SC transplantation significantly improves the survival of host neurons and promotes the regeneration of 5-hydroxytryptamine-positive and calcitonin gene-related peptide-positive axons (Guo et al., 2007). Accordingly, SCs are widely used in studies of SCI repair.

Neurotrophin-3 (NT-3) plays an important role in the development and differentiation of neurons, as well as the survival of injured central neurons and the regeneration of axons (Elliott Donaghue et al., 2015; Zhang et al., 2016). In a study that used a subacute model of SCI, the controlled release of silk fibroin NT-3 enhanced the growth of nerve fibers crossing the glial scar interface (Johnson et al., 2009). In another study, a large number of nerve stem cells (NSCs) overexpressing NT-3 differentiated into neurons expressing the marker microtubule associated protein-2 when cultured on three-dimensional biomaterials. In contrast, NSCs that were not genetically modified in the control group mainly differentiated into astrocytes (Xiong et al., 2009). Furthermore, previous studies have shown that NT-3 promotes the functional maturation and remyelination of oligodendrocytes (Ding et al., 2015; Qiu et al., 2015).

The safety and effectiveness of a variety of biomaterials, including agarose, collagen, gelatin, chitosan, fibronectin and hyaluronic acid, have been investigated in preclinical studies (Bozkurt et al., 2010; Günther et al., 2015; Liu et al., 2017). In the past 10 years, collagen sponge has been the most widely used bioscaffold for the repair of SCI. However, the distribution of transplanted cells in this scaffold is random and disordered, with non-directional regeneration of host axons. Given its importance, a bioscaffold that facilitates directional axon regeneration in SCI lesions is essential (Deng et al., 2021). In a previous study, we found that decellularization can optimize the normally non-permissive microenvironment in adult porcine optic nerve to facilitate the oriented outgrowth of dorsal root ganglion (DRG) neurites *in vitro* (Sun et al., 2020). However, whether a decellularized optic nerve (DON) scaffold promotes *in vivo* directional axon regeneration is unknown. Hence, in this study, we investigated the use of a DON functional scaffold containing NT-3-overexpressing SCs (SCNTs) to support the directional regeneration of axons and promote remyelination for the repair of dorsal white matter SCI.

Materials and Methods

Scaffold preparation

All procedures involving animals were conducted in accordance with the ethical standards of the Institutional Animal Care and Use Committee of Sun Yat-sen University (approval No. SYSU-IACUC-2019-B034, approved on February 28, 2019) and the National Institutes of Health Guide for the Care and Use of Laboratory Animals. All experiments were designed and reported according to the Animal Research: Reporting of *In Vivo* Experiments (ARRIVE) guidelines. Decellularized nerve scaffolds were prepared as described previously (Sun et al., 2020). Briefly, fresh optic nerve and sciatic nerve were collected from adult pigs (~2 years of age, supplied by Northwest Agriculture and Forestry University, China). Cellular components in two nerves were sequentially extracted with 3% Triton X-100 (Amresco, Solon, OH, USA), 4% sodium deoxycholate (Sigma-Aldrich, St. Louis, MO, USA), 50 U/mL DNase (Sigma-Aldrich) and 10 μg/mL RNase (Sigma-Aldrich) on a shaker (Allsheng OS-100, Hangzhou, China). Then, de-fatting processes were performed on the sciatic nerve. All processes were performed under sterile conditions. The porcine DON scaffold and decellularized sciatic nerve (DSN) scaffold were freeze-dried for 24 hours and then stored at 4°C until use (for up to 1 month). Commercial collagen sponge (CS, BIOT Biology, Wuxi, China) as a scaffold material was also used, for comparison, as described below.

Identification and optimization of scaffold

A total of five sections of each scaffold (n = 3) were selected. Hematoxylin and eosin staining and scanning electron microscopy were used to assess the crosswise and longitudinal scaffold structures of the different groups. After immunofluorescence staining for chondroitin sulfate proteoglycans (CSPGs), laminin (LN) or collagen IV (COL4), four images of random fields of each scaffold section (four corners) were captured under a microscope (DM6B, Leica, Wetzlar, Germany) at a typical magnification of 100×. The mean intensity of positive immunofluorescence was determined using ImageJ software (National Institutes of Health, Bethesda, MD, USA).

Seeding of NSCs and assessment of cell viability

Each scaffold was shaped into a short column (3 mm in diameter and 2 mm in length). NSCs were isolated from Sprague-Dawley rats (n = 18, Experimental Animal Center of Sun Yat-sen University (license No. SCXK (Yue) 2016-0029), Guangzhou, China), as described previously (Zeng et al., 2005). Briefly, rats at postnatal day 1 (P1) were anesthetized with aether, and the hippocampus was mechanically dissected and dissociated into a single-cell suspension. The cells were cultured in Dulbecco's modified Eagle's medium (DMEM)/F12 (Hyclone, Logan, UT, USA) containing 1% B27 (Life Technologies, Carlsbad, CA, USA) and 20 ng/mL basic fibroblast growth factor (Life Technologies). After 7 days, the cells grew as neurospheres in suspension. Nestin immunoreactivity was assessed and confirmed for all neurospheres. A total of 2×10^5 NSCs in 20 μL culture medium were seeded onto each scaffold (n = 9 in each group). The cell/scaffold mixture was maintained in DMEM/F12 (1:1) supplemented with 1% B27 and 2% fetal bovine serum for another 7 days. For cell viability, Cell Counting Kit-8 assay (Saint-Bio, Shanghai, China) was performed according to the manufacturer's instructions. Briefly, the reagent was incubated with the NSC-seeded scaffolds for 4 hours in an atmosphere of 5% CO_2 at 37°C. The culture plate was shaken for 20 minutes to allow complete dye dissolution, and then the solution from each scaffold was transferred to another well and this process was repeated three more times. Cell viability was assessed using an absorbance reader (Sunrise, Tecan, Grödig, Austria). The optical density of each sample was measured at 450 nm, and a cell viability chart was drawn.

DRG culture on the scaffolds

DON, DSN and CS scaffolds were cut into 200-μm-thick slices (3 mm in width and 4 mm in length, n = 5 for each group). DRGs with dorsal roots were dissected from green fluorescent protein (GFP) transgenic P1 rats and collected in cold DMEM/F12 medium, and then redundant dorsal roots were removed under a stereomicroscope. Fifteen DRGs were placed on 15 slices and cultured with DMEM/F12 medium containing 2% B27, 2% fetal bovine serum, 0.3% L-glutamine and 100 ng/mL NGF in a 37°C incubator with 5% CO_2. The medium was

changed every day. After 3 days of culture, the DRGs were fixed with 4% paraformaldehyde in phosphate-buffered saline (PBS). To evaluate DRG neurites, we measured the length and area of neurofilament (NF)-positive (NF^+) neurites, and quantified the percentage of directional neurites manually under a microscope. To this end, we measured the proportions of neurites with ranging angle of 0–30° between the NF-positive neurites and the longitudinal axis of the scaffold slice. To assess the myelination potential of the three scaffolds, we observed the number of myelin basic protein (MBP)-positive (MBP^+) SCs attached to NF-positive neurites and quantified them under a fluorescent microscope. After 14 days of culture, the DRGs were fixed for ultrastructural observation of the myelin structure under a transmission electron microscope (Philips CM 10, Amsterdam, Netherlands).

Functional scaffold preparation

SCs were obtained from 7-day-old GFP transgenic Sprague-Dawley rats (*n* = 12, Osaka University, Osaka, Japan), as described previously (Zeng et al., 2005). Briefly, sciatic nerves and the brachial plexus were dissected, and the connective tissue was removed under a stereomicroscope. All nerves were cut into small pieces (< 1 mm) and dissociated with 0.16% collagenase (Sigma-Aldrich). SCs were cultured with DMEM/F12 containing 10% fetal bovine serum, 2 μM forskolin (Sigma-Aldrich) and 20 mg/mL bovine pituitary extract (Sigma-Aldrich), and passaged at 90% confluence. The cells were then purified using differential adhesion and digestion techniques. The cells were transfected with an adeno-associated viral vector carrying the NT-3 (NM_002527, Vigene Biosciences, Rockville, MD, USA) coding sequence for 12 hours. The scaffolds were manually shaped into an appropriate dimension (1 mm width × 1 mm height × 2 mm length) using a blade. A total of 1×10^5 SCNTs in 10 μL culture medium were seeded into every scaffold, and then incubated for 3 days. Rabbit anti-NT-3 and rabbit anti-S100 antibodies were used for identification of SCNTs.

Spinal cord surgery and transplantation

Adult female Sprague-Dawley rats (200–250 g, supplied by the Experimental Animal Center of Sun Yat-sen University) were randomly assigned to the following two groups: DON scaffolds containing SCNTs (DON group, *n* = 12) and CS scaffolds containing SCNTs (CS group, *n* = 10) (22 rats in total). Half of the animals from each group were used for immunofluorescence analysis, while the remaining half were used for structural observation of remyelination. Three days before surgery, all animals were given cyclosporine A (Novartis Pharma Schweiz AG, Eberbach, Germany) by subcutaneous injection (1 mg/100 g per rat). The animals were anesthetized with 1% pentobarbital sodium (40 mg/kg). A laminectomy was performed at the T9 vertebral level to expose the T10 spinal segment, and the dura was vertically cut with microdissection scissors. Bilateral incisions were made 0.5 mm from the dorsal midline of the spinal cord to form a rectangular gap (1 mm in width, 1 mm in depth, and 2 mm in length) in the T10 segment. Then, functional scaffolds of the same size were used to fill the gaps in each group. All rats received extensive post-surgery care, including intramuscular injection of penicillin (50,000 U/kg per day) for 3 days, and manual voiding was performed twice per day until automatic micturition function was reestablished. The cyclosporine A was administrated once a day for 4 weeks.

Tissue preparation

All rats were deeply anesthetized with 1% pentobarbital sodium (50 mg/kg, intraperitoneally) and intracardially perfused with physiological saline containing 0.002% $NaNO_2$ and 0.002% heparin, followed by 4% paraformaldehyde. After perfusion, the spinal cord was dissected, postfixed overnight in the same fixative, and dehydrated in 30% sucrose/PB. For immunofluorescence staining, longitudinal sections of the selected spinal cord segments were cut at 25 μm thickness using a cryostat, and all sections were stored at −30°C until further processing. The remaining segments were dissected for structural observation of remyelination.

Ultrastructural observation of remyelination

All three scaffolds (DON, DSN and CS) *in vitro* were coated with gold and examined by scanning electron microscopy (Philips XL30 FEG). For ultrastructural observation of remyelination under a transmission electron microscope (Philips CM 10), the *in vitro* DRG cultures and the *in vivo* spinal cord segments containing a functional scaffold were post-fixed in fixative solution containing 2.5% glutaraldehyde and 4% paraformaldehyde overnight at 4°C. The samples were then washed in PBS, dehydrated through a graded ethanol series, and flat-embedded in Epon812 (TED PELLA, Redding, CA, USA). For *in vivo* quantification, semi-thin sections of spinal cord segments were cut using a Leica RM2065 microtome, stained with toluidine blue (5% in a borax solution), and mounted on glass slides. Three semi-thin sections were selected from the injury/graft site of the spinal cord of each rat for remyelination analysis. Nine sections were selected from each group of three animals. Three regions of interest were selected in each section and examined at 1000× magnification. Newborn myelin sheaths (thin sheaths and light in color) were counted and compared between the two groups. Ultrathin sections (100 nm in thickness) of the DRG cultures and the injury/graft site of the spinal cord were cut, double-stained with lead citrate and uranyl acetate, and examined under the transmission electron microscope.

Immunofluorescence staining

The sections were rinsed with 0.01 M PBS three times, blocked with 10% goat serum for 30 minutes, and incubated with primary antibodies in 0.3% Triton X-100 overnight at 4°C. After rinsing with PBS, the sections were incubated with the secondary antibodies for 1 hour at 37°C and Hoechst 33342 (Invitrogen, Carlsbad, CA, USA) and examined under the fluorescence microscope (DM6B, Leica). A summary of antibodies used is provided in **Additional Table 1**.

Morphological quantification

For *in vitro* quantification, a total of five sections from each scaffold were selected (*n* = 5 in each group). Four images of random fields of each scaffold section (four corners) were captured under the microscope (DM6B, Leica) at a typical magnification of 100×. The total area showing the mean intensity of positive immunofluorescence was determined using ImageJ software.

For *in vivo* quantification, we conducted staining for mouse antibody to NF to identify regenerated axons and to quantify the percentage of directional neurites under a microscope. Chicken anti-MBP antibody staining was performed to identify the myelin sheath. Mouse anti-ionized calcium binding adaptor molecule 1 (IBA-1) antibody staining was performed to assess the inflammatory response. Rabbit anti-CSPGs antibody was used to identify extracellular matrix (ECM). Selected sections (*n* = 5 in each group) were further analyzed with a confocal (Dragonfly) microscope and iMaris software (Oxford Instruments, Oxford, UK). NF- and MBP-positive areas were quantified in lesions for comparisons of the different groups. Directional axon regeneration was quantified according to the proportions of neurites with ranging angle of 0°–30° between the NF-positive axon and the longitudinal axis of the spinal cord. The number of IBA-1-positive (IBA^+) cells was quantified in the rostral and caudal areas, and within each lesion, for comparisons among the different groups. CSPGs-positive ($CSPG^+$) areas (360 μm × 360 μm) were calculated and compared in the same way.

Statistical analysis

Data were analyzed using SPSS 20.0 software (IBM Corp.,

Armonk, NY, USA). Comparisons between samples were evaluated by one-way analysis of variance and the least statistical difference test. Differences were considered statistically significant at $P < 0.05$. All values are expressed as mean ± standard deviation (SD).

Results

Characterization of DON, DSN and CS scaffolds

Both DON and DSN were processed from fresh porcine nervous tissue. The DON scaffold with many longitudinal channels and a three-dimensional topographic structure was prepared from fresh optic nerves decellularized using a chemical extraction method and a vacuum freeze-drying process (**Figure 1A–D**). Transverse and longitudinal scaffold sections were evaluated after hematoxylin and eosin staining. The DON scaffold showed uniformly distributed straight channels with uniform hole sizes (**Figure 1E1** and **F1**). The DSN scaffolds had straight longitudinal channels, but the holes were not of uniform size (**Figure 1E2** and **F2**). Compared with holes in transverse sections, the shorter channels in longitudinal sections showed no structural differences in the CS, and they were still randomly distributed, which can provide a larger cell-attachment surface (**Figure 1E3** and **F3**).

Next, we characterized the topographic structure of each scaffold using scanning electron microscopy (**Figure 1G1–H3**). The horizontal holes of the DON scaffold were evenly distributed, and the longitudinal channels were straight. Additionally, there were a few pore structures connecting the individual longitudinal channels (**Figure 1G1** and **H1**). In the DSN scaffold, the distribution of the channel and hole structures in longitudinal and transverse sections was relatively non-uniform (**Figure 1G2** and **H2**), and in the CS scaffold, they were random and disordered (**Figure 1G3** and **H3**). These results suggest that the DON scaffold has the structural basis for guiding the directional outgrowth of neuronal axons, and at the same time, to allow the exchange of information (cues) between channels, which is conducive to axonal communication and cell migration.

Levels of specific ECM proteins in DON, DSN and CS scaffolds

Before assessing the effects of the three kinds of scaffolds on DRG neurite outgrowth, we quantitatively measured the levels of relevant ECM proteins on each scaffold. To this end, we selected three major ECM proteins associated with neurite growth—CSPGs, LN and COL4. CSPGs were rarely detected on the DON and CS scaffolds, whereas the DSN scaffold exhibited the highest immunofluorescence for CSPGs (**Figure 2A–C** and **Additional Figure 1A–C**). The distributions of LN and COL4 were notably different among the scaffolds. The DON had the highest fluorescence staining for LN and COL4, followed by the DSN, with the CS having the least staining (**Figure 2D–I** and **Additional Figure 1D–I**). These results indicate that the DON scaffold contains abundant LN and COL4 (**Figure 2J**), which may promote neurite growth, but barely any CSPGs, which inhibit neurite growth.

Viability of NSCs in DON, DSN and CS scaffolds *in vitro*

Before being seeded onto the scaffolds, Nestin immunoreactivity was confirmed for all neurospheres. To determine whether the NSCs on each scaffold were viable, they were seeded and cultured for 7 days. The Cell Counting Kit-8 analyses showed that NSCs grew better and displayed better viability on the DON and CS scaffolds than on the DSN scaffold ($n = 9$ in each group, $P < 0.05$; **Figure 2K**). These results suggest that the DON and CS scaffolds can provide better structural support for NSCs adherence and growth.

DRG neurite outgrowth on DON, DSN and CS scaffold slices *in vitro*

Next, the ability of each scaffold to support neurite extension was examined using the DRG culture model. All DON slices were placed at the bottom of a 24-well culture plate, and freshly isolated DRG cells were seeded on them and cultured for 3 days. DSN and CS slices were used as controls. The cultures were stained for NF by immunofluorescence, and the maximum distance of DRG neurite extension was measured (**Figure 3A–C**). All scaffolds supported robust NF-positive neurite extension (**Figure 3D–F**), but the neurites on the DON scaffold were the longest (**Figure 3A** and **G**), followed by the DSN (**Figure 3B** and **G**) and then the CS (**Figure 3C** and **G**; $n = 5$ in each group, $P < 0.01$). The total area showing DRG NF-positive neurite extension had similar characteristics (**Figure 3G** and **H**), and the DON and DSN scaffolds showed the best directional growth of neurites ($n = 5$ in each group, $P < 0.01$; **Figure 3I**). These results indicate that the DON and DSN scaffolds promote the directional growth of DRG neurites.

DON scaffolds have more SCs adhering to DRG neurites *in vitro*

Next, we evaluated the potential of each scaffold to support neurite myelination using the DRG culture system. To distinguish between DRG neurites and SCs, the cultures were immunostained for NF and MBP. Most SCs adhered to NF-positive neurites on the DON scaffold, followed by the DSN and CS scaffolds ($n = 5$ in each group, $P < 0.05$; **Figure 3J**). Next, the wrapping of SCs around DRG neurites was investigated by transmission electron microscopy. After culture for 2 weeks, SCs were observed on the DON scaffold, which appeared to feature different stages of myelination, including a multilayer myelin sheath structure and early myelinated neurites (**Figure 3K** and **L**). These results suggest that the DON scaffold may be better able to promote myelination of SCs on neurites, compared with the DSN and CS scaffolds.

The DON functional scaffold enhances directional axon regeneration and remyelination

In the present study, both the DON and CS scaffolds contained SCNTs. The transfection rate of the NT-3 gene in cultured SCNTs exceeded 80%, and the SCNTs were positive for S100 protein (**Figure 4A** and **B**), indicating that the modified SCNTs were suitable for loading onto these scaffolds. Next, these scaffolds were transplanted into SCI lesions of the dorsal white matter (**Figure 4C**). Four weeks later, the distribution of grafted SCNTs in lesions better paralleled the longitudinal axis of the spinal cord in the DON group (**Figure 5A** and **C1**), compared with the CS group (**Figure 5B** and **D1**). In addition, the directional regeneration of host axons in lesions was consistent with the longitudinal axis of the spinal cord (**Figure 5C**, **C2** and **G**). In contrast, in the CS group, the regenerated axons in lesions grew in a disordered manner (**Figure 5D**, **D2** and **G**). At the same time, the quantification of axons and myelin revealed more NF and MBP expression in lesions in the DON group (**Figure 5C–F**), compared with the CS group. To verify the effects of the functional scaffolds on axon remyelination, myelin sheath analysis was performed. In lesions in the DON group, most regenerated axons were wrapped with new myelin sheaths, whereas in the CS group, few axons were wrapped in such a manner (**Figure 6A–D**). Transmission electron microscopy analyses confirmed these results (**Figure 6E** and **F**).

The DON functional scaffold alleviates inflammation and reduces CSPGs levels

At 4 weeks after SCI, IBA-1-positive cells and CSPGs level were evaluated in the DON and CS groups (**Figure 7A**). There were more IBA-1-positive cells in lesions in the CS group, compared with the DON group ($P < 0.05$; **Figure 7B1–C3**). Transplantation with the DON scaffold decreased the number of IBA-1-positive cells in the areas rostral and caudal to the lesion, as well as within the lesion, compared with the CS group ($P < 0.05$; **Figure 7F**). CSPGs levels in these areas were lower in the DON group than in the CS group ($P < 0.05$; **Figure 7D1–E3** and **G**). Therefore, these results indicate that the transplanted DON scaffold containing SCNTs attenuates inflammation and lowers CSPGs levels.

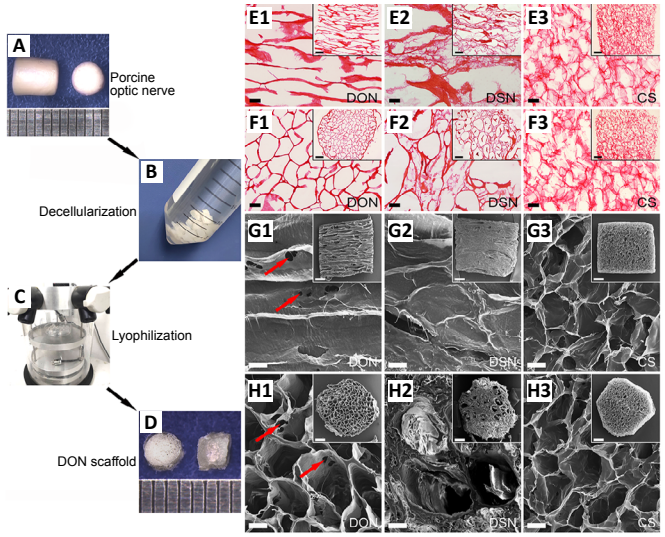

Figure 1 | Preparation and structural characterization of decellularized scaffolds.
(A–D) A schematic diagram of the decellularization process for the DON scaffold. Fresh porcine optic nerve tissue (A) was subjected to decellularization by chemical extraction (B) and lyophilization (C). DON with a diameter of about 3 mm is shown on the left (D). (E1–F3) Hematoxylin and eosin staining showing the structures of longitudinal sections of DON (E1), DSN (E2) and CS (E3), and transverse sections of DON (F1), DSN (F2) and CS (F3). (G1–H3) Scanning electron microscopy showing the three-dimensional spatial structure in longitudinal sections of DON (G1), DSN (G2) and CS (G3), and transverse sections of DON (H1), DSN (H2) and CS (H3). Some pores (H1, red arrows) were observed on the walls of the longitudinal channels in the DON scaffold. The DON scaffold showed uniformly distributed straight channels with uniform hole sizes in comparison with other two groups. Scale bars: 100 μm in E1–H3, and 500 μm in illustrations of E1–H3. CS: Collagen sponge; DON: decellularized optic nerve; DSN: decellularized sciatic nerve.

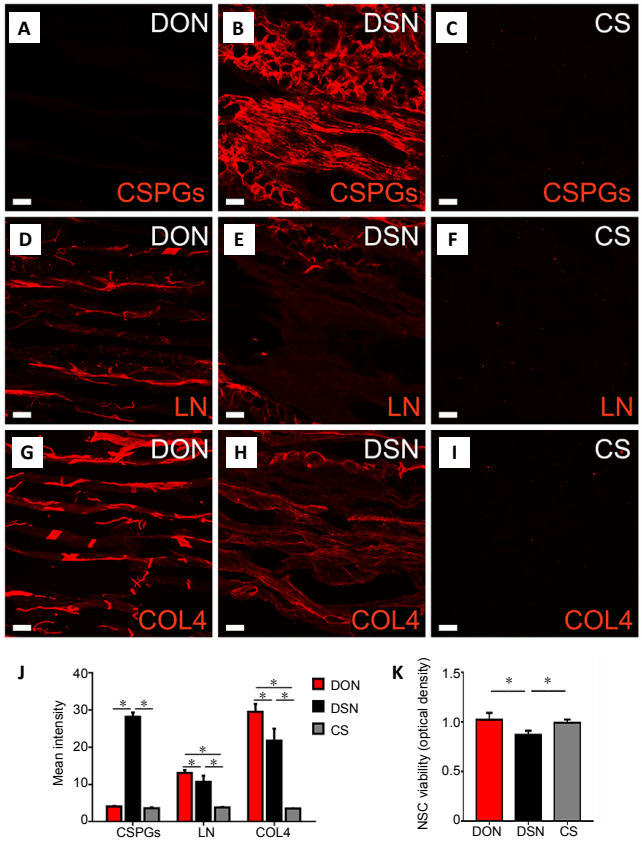

Figure 2 | ECM proteins and their impact on the viability of NSCs in the scaffolds.
(A–I) Distribution of CSPGs (A–C), LN (D–F) and COL4 (G–I) on the DON, DSN and CS scaffolds. Scale bars: 60 μm in panels. (J) Immunoreactivity for CSPGs, LN and COL4 in the DON, DSN and CS scaffolds. Positive CSPGs immunoreactivity was detected in the DSN, but barely in the DON and CS. The DON had the highest immunofluorescence staining for LN and COL4, followed by the DSN, with the CS having the least staining. (K) Effects of the DON, DSN and CS scaffolds on NSC viability by Cell Counting Kit-8 analysis. Data are presented as mean ± SD (n = 5). *P < 0.05 (one-way analysis of variance followed by the least statistical difference test). COL4: Collagen IV; CS: collagen sponge; CSPGs: chondroitin sulfate proteoglycans; DON: decellularized optic nerve; DSN: decellularized sciatic nerve; ECM: Extracellular matri; LN: laminin; NSCs: neural stem cells.

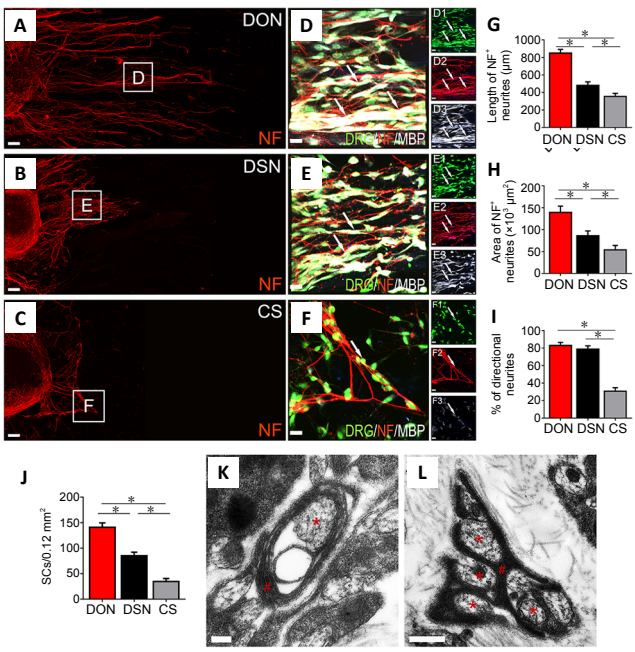

Figure 3 | Effects of DON, DSN and CS scaffolds on neurite outgrowth and myelination.
DRGs were seeded on the scaffold slices and cultured for 3 days. (A–C) Showing NF-positive neurite (red) growth on the DON, DSN and CS scaffold slices. (D–F) Enlarged images of the areas in the squares in panels (A–C). NF-positive neurites were adhered by MBP-positive SCs (white) perfectly under the fluorescence microscope (D–F, D1–F3). (G, H) The length and area of neurites on the DON scaffold were the largest, followed by the DSN and then the CS. (I, J) The percentage of directional growth of neurites (I) and number of SCs (J). (K, L) The DON scaffold slice under the transmission electron microscope following 14 days of culture with DRGs *in vitro*. The neurites (red asterisks) were perfectly wrapped by SCs (red pounds). The data are presented as mean ± SD (n = 5). *P < 0.05 (one-way analysis of variance followed by the least statistical difference test). Scale bars: 100 μm in A–C, 20 μm in D–F, 20 μm in D1–F3, 200 nm in K, 500 nm in L. CS: Collagen sponge; DON: decellularized optic nerve; DRG: dorsal root ganglion; DSN: decellularized sciatic nerve; MBP: myelin basic protein; NF: neurofilament; SCs: Schwann cells.

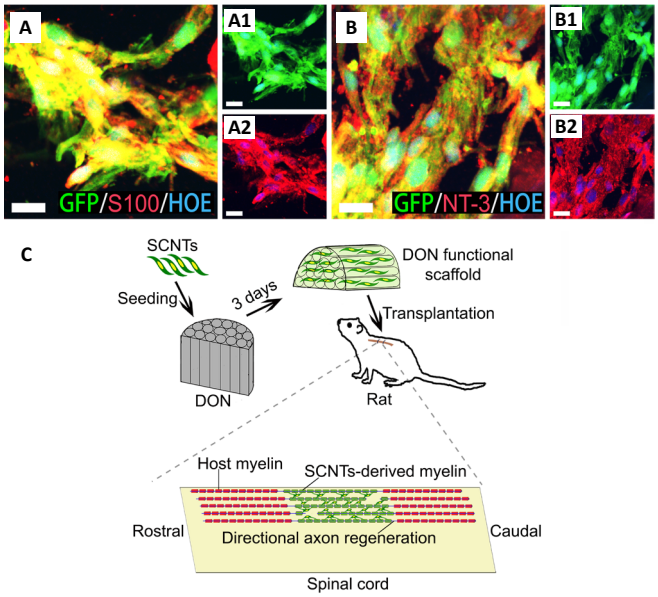

Figure 4 | DON functional scaffold construction and transplantation.
(A, B) S100-positive SCNTs (A, A1, A2) and NT-3-positive SCNTs (B, B1, B2) in the DON functional scaffold (red fluorescence) at 3 days of culture. Scale bars: 20 μm in panels. (C) A schematic diagram of construction and transplantation of the DON functional scaffold. DON: Decellularized optic nerve; GFP: green fluorescent protein; HOE: Hoechst33342; NT-3: neurotrophin-3; SCNTs: NT-3-overexpressing Schwann cells.

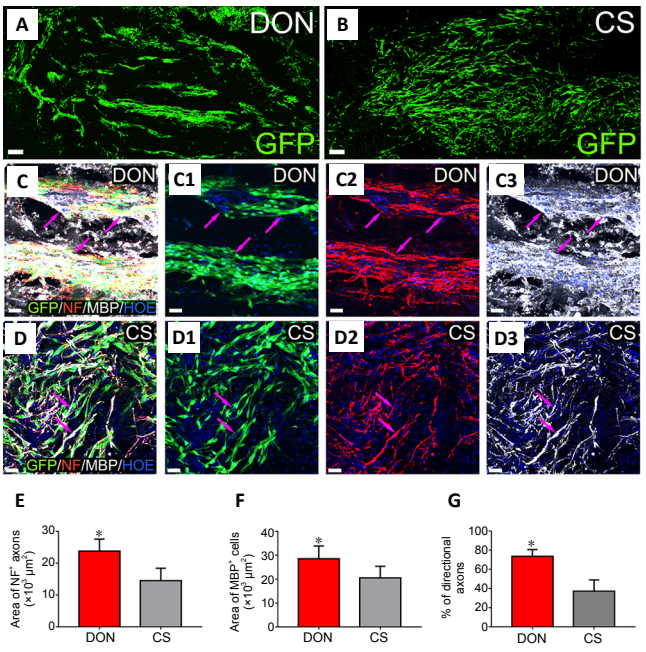

Figure 5 | **Axonal regeneration and remyelination in lesions of the dorsal white matter of the spinal cord after transplantation of the functional scaffolds.**

(A, B) Distribution of GFP-positive grafted SCNTs in the DON (A) and CS (B) functional scaffolds in lesions. (C–D3) GFP-positive donor cells expressing MBP and NF-positive axons (red) adhered by MBP-positive SCNTs (white) in the DON (C–C3, purple arrows) and CS (D–D3, purple arrows) functional scaffolds in lesions. Scale bars: 100 μm in A and B, and 30 μm in C–D3. (E, F) Areas of NF-positive axons (E), MBP-positive area (F), and the percentage of directional axon regeneration (G) in lesions in the DON and CS groups. The data are presented as mean ± SD (n = 5). *P < 0.05, *vs.* CS (one-way analysis of variance followed by the least statistical difference test). CS: Collagen sponge; DON: decellularized optic nerve; GFP: green fluorescent protein; MBP: myelin basic protein; NF: neurofilament; SCNTs: neurotrophin-3-overexpressing Schwann cells.

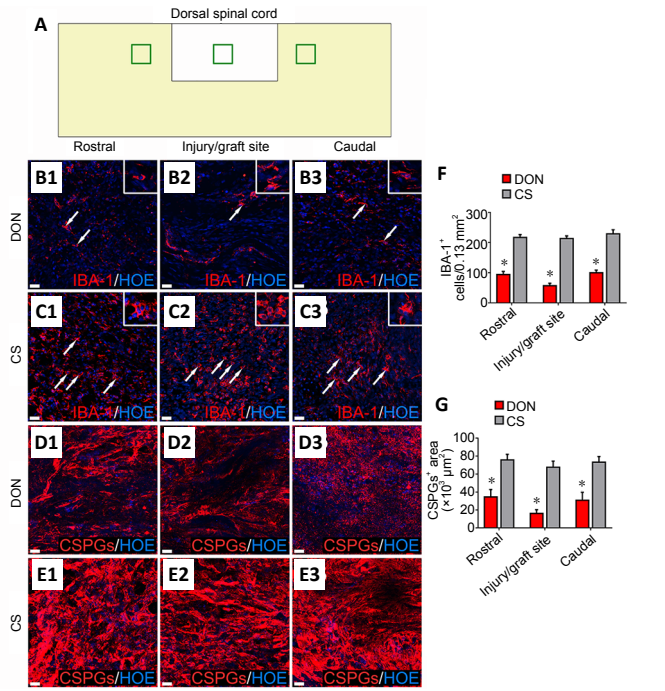

Figure 7 | **Effects of functional scaffolds on the inflammatory cells and CSPGs levels in the injured spinal cord.**

(A) A diagram showing sampling sites in a longitudinal section of injured spinal cord. (B1–B3) IBA-1-positive cells (white arrows) in the rostral (B1), injury/graft (B2) and caudal (B3) sites of spinal cord in the DON group. (C1–C3) IBA-1-positive cells (white arrows) in the rostral (C1), injury/graft (C2) and caudal (C3) sites in the CS group. (D1–E3) CSPGs immunofluorescence in longitudinal sections of the injured spinal cord. Fewer IBA-1-positive cells and lower CSPGs expression were found in the DON group compared with the CS group. Scale bars: 30 μm in B1–E3. (F) Number of IBA-1-positive cells in the DON and CS groups. (G) Level of CSPGs in the DON and CS groups. The data are presented as mean ± SD (n = 5). *P < 0.05, *vs.* CS (one-way analysis of variance followed by the least statistical difference test). CS: Collagen sponge; CSPGs: chondroitin sulfate proteoglycans; DON: decellularized optic nerve; HOE: Hoechst 33342; IBA-1: ionized calcium binding adaptor molecule 1.

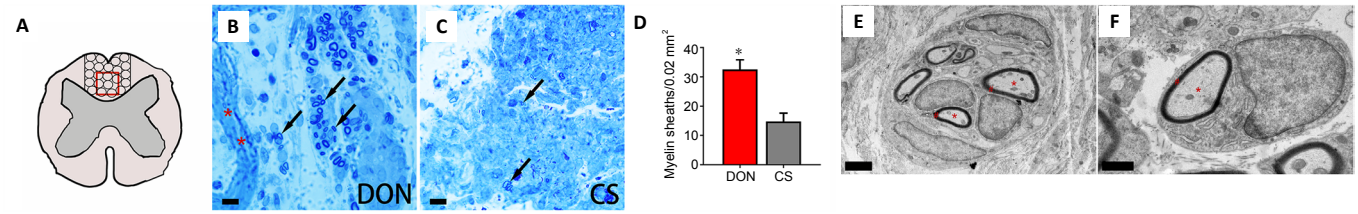

Figure 6 | **Impact of functional scaffolds on newborn myelin sheaths in lesions in the spinal cord.**

(A) A schematic diagram showing the location (red squares) of myelin sheath counting in dorsal white matter injury/graft site of spinal cord. (B, C) Many newborn myelin sheaths (B, dark arrows) are visible in semi-thin sections stained by toluidine blue in the DON group, and a few newborn myelin sheaths (C, dark arrows) are visible in the CS group. (D) The number of newborn myelin sheaths in lesions of the spinal cord in the two groups. The data are presented as mean ± SD (n = 3). *P < 0.05, *vs.* CS (one-way analysis of variance followed by the least statistical difference test). (E, F) Transmission electron microscopy showing that the regenerating axons (red asterisks) were enwrapped by newborn myelin sheath (red hashes, showing a thin layer myelin sheath) in lesions of the spinal cord in the DON group. Scale bars: 10 μm in B and C, 2 μm in E, 1 μm in F. CS: Collagen sponge; DON: decellularized optic nerve.

Discussion

Improving the local microenvironment in SCI lesions to promote axonal regeneration and activate the intrinsic axon regenerative potential of injured neurons are key objectives in the treatment of SCI (Bartholomew, 1988; Zhao et al., 2013). As tissue engineering, genetic engineering, and stem cell techniques have advanced over the past two decades, scientists have been able to improve the microenvironment at the site of injury and induce substantial axon regeneration by delivering a cocktail of neurotrophins through transplantation of ECM and stem cells (Lu et al., 2014; Mukhamedshina et al., 2019; Liu et al., 2020). However, effectively enhancing directional axon regeneration after white matter injury and promoting regenerative axon myelination remain major challenges (Unal et al., 2019; Cao et al., 2020).

Tissue engineering is a novel treatment approach developed in recent decades that has advanced rapidly with progress in functional biomaterials, genetic engineering, and stem cell technologies (Cheng et al., 2020; Tsintou et al., 2020). All neuronal axons in the white matter run parallel to the long axis of the spinal cord. Therefore, a tissue engineering bioscaffold for spinal cord white matter repair should encourage the correct directional growth of axons (Deng et al., 2021). In addition, the homeostasis of the microenvironment of a scaffold can be better maintained if its components are more similar to those of ECM tissue (Unal et al., 2019). Studies have shown that DSN tissue and decellularized spinal cord tissue have more components similar to the ECM in the nervous system than synthetic scaffold materials, and they can provide a stable microenvironment for axon regeneration and myelination (Buckenmeyer et al., 2020). In fact, the proteins of

the ECM in decellularized spinal cord are most similar to those in normal spinal cord. However, the decellularized spinal cord, initially a tube-like structure, collapses after decellularization, which affects cell loading and axonal regeneration (Zeng et al., 2011; Xing et al., 2019). Our research group has found that the DON scaffold has the potential to direct the regenerative growth of DRG neurites (Sun et al., 2020). In this study, we evaluated the DON, DSN and CS scaffolds to identify the one that is more suitable for maintaining the homeostasis of the microenvironment for nerve regeneration and remyelination.

Hole sizes in the CS were similar to those of the DON scaffold, but they were unevenly arranged in a sponge-like structure. Both DON and DSN scaffolds had straight channels, and channel collapse was not observed after decellularization. The three-dimensional structures of the scaffolds under a scanning electron microscope were similar to those of HE-stained sections. More importantly, 20–50-μm pores were present in the walls of the straight channels in longitudinal sections of the DON scaffold. Between the straight channels, these naturally arranged pores may facilitate the migration of seeded cells, contact among neural processes, and communication between neurotrophins, which is not possible with existing three-dimensional printed bioscaffolds (Bartholomew, 1988; Joung et al., 2018; Kaplan et al., 2020). The holes on the transverse section of the DON were approximately similar to those in the CS. However, those in the DSN were unevenly arranged. It is important that the pores and/or channels and their distribution in the DON and CS scaffolds help increase the surface area for the attachment of seeded cells.

A previous study showed that the DON scaffold contains a number of ECM components that help guide the regeneration of axons (Sun et al., 2020), whereas the DSN contains more ECM components that promote myelination. We examined the proteins in the ECM of each scaffold, and found that the internal surface of the channels of the DON contains a large amount of LN and COL4, which enhance DRG neurite outgrowth (Hosseinkhani et al., 2013; Sun et al., 2020). CSPGs inhibiting DRG neurite outgrowth in the DON were significantly reduced compared with the DSN. The DSN scaffold contained lower levels of LN and COL4 than the DON. The CS scaffold had the lowest levels of LN, COL4 and CSPGs. These results suggest that the DON scaffold promotes axonal regeneration, and that the CS may neither promote nor inhibit this process. When the same number of NSCs were seeded into each scaffold, they showed better viability in the DON and CS scaffolds than in the DSN, probably because the bigger hole diameter of the DSN affects the adhesion and survival of NSCs. In addition, the DSN microenvironment featuring a large number of CSPGs may also lead to the lower viability of NSCs (Hussein et al., 2020).

To further verify the effects of the DON, DSN and CS scaffolds on directional axon regeneration and myelination, a model of *ex vivo* cultured DRGs was designed and produced. After 3 days of *in vitro* DRG culture, a mass of SCs was observed migrating out from the DRG tissue, and many NF-positive neurites also appeared. The DON scaffold helped guide NF-positive neurites growing along the straight channels. At the same time, many SCs adhered to the neurites. The channels in the DSN also helped guide the directional regeneration of NF-positive neurites. However, fewer and shorter NF-positive neurites were observed, compared with the DON scaffold. In addition, fewer SCs adhered to NF-positive neurites and more SCs were randomly distributed. The CS was inferior in all aspects. When the culture time of the DRGs was prolonged to 14 days, the DON scaffold promoted the formation of myelinated neurites. These encouraging results obtained with the DON scaffold warrant *in vivo* experiments to assess its effectiveness for treating SCI.

Previous studies have shown that NT-3 can promote the survival of transplanted cells and host neural cells, the regeneration of host neuronal axons, and the myelination of SCs in SCI lesions (Lai et al., 2019; Smith et al., 2020). Many studies have demonstrated that SCs can form myelin sheaths around regenerating axons and also secrete multiple neurotrophic factors to improve the microenvironment at the site of tissue damage following SCI (Walker et al., 2015; Lai et al., 2016; Walker and Xu, 2018). Therefore, we posited that a DON loaded with SCNTs could act as a tissue engineering functional scaffold to promote directional axon regeneration and myelination to repair white matter SCI. To test this, we created a rat model of dorsal white matter SCI and treated the rats with DON functional scaffolds. We found that, 4 weeks after transplantation, SCNTs in these scaffolds survived well; a large number of donor SCNTs were distributed along the straight channels, and many regenerated axons had become remyelinated with donor SCNTs. Hence, this scaffold showed good directional axon regeneration and myelination. This may be due not only to its channels, which help guide axonal regeneration and myelination, but also to its suitable microenvironment, as this scaffold showed low levels of inflammation and had few CSPGs (Orr and Gensel, 2018; Stephenson and Yong, 2018). These data further indicate that DON functional scaffolds would integrate well with host spinal cord tissues. However, it is necessary for further research to perform anterograde/retrograde tracing to better identify the regenerating axons.

More broadly, our results demonstrate the importance of the physical channels and microstructure (with some micro-scale pores located in the walls of the channels) to facilitate neural cell growth and function (Bedir et al., 2020; Yang et al., 2020). In addition, this study emphasizes the importance of the source of the scaffold material and the microenvironment created by the ECM in maintaining the viability of the seeded cells, thereby creating a tissue engineering functional scaffold that promotes axonal regeneration and myelination (Rao and Pearse, 2016; Cerqueira et al., 2018; Liu et al., 2020). However, the role of chemoattractants, such as NT-3 or netrin in promoting directional axon growth should be further investigated.

In conclusion, we describe here a novel tissue-engineering strategy for the repair of white matter SCI. In view of the clinical need for efficient white matter repair, it is necessary to further explore the mechanisms of nerve regeneration and myelination to optimize the DON-derived functional scaffold. Future studies should modify the ECM proteins on the scaffold and evaluate animal behavior and electrophysiological function in detail, as well as carry out experiments in large animal models to test efficacy in preclinical application. The DON scaffold can also be loaded with other types of functional seed cells, such as iPSC-derived neural cells, and it could be shaped and functionally modified according to the characteristics of the specific nervous tissue being repaired.

Author contributions: *Conception and design of the study: YSZ, BQL; experiment implementation and data collection: YRB, BQL, WTH, JHS, GL, YHM; analysis and interpretation of the data: YRB, BQL, YSZ, YD, XZ; manuscript drafting: YRB, BQL, YSZ. All authors approved the final version of the manuscript.*
Conflicts of interest: *The authors declare no conflict of interest.*
Financial support: *This work was supported by grants from the National Key R&D Program of China, No. 2017YFA0104704 (to BQL); the Young Elite Scientist Sponsorship Program (YESS) by China Association for Science and Technology (CAST), No. 2018QNRC001 (to BQL); the Fundamental Research Funds for the Central Universities, China, No. 18ykpy38 (to BQL); and the National Natural Science Foundation of China, Nos. 81971157 (to BQL), 81891003 (to YSZ). The funding sources had no role in study conception and design, data analysis or interpretation, paper writing or deciding to submit this paper for publication.*
Institutional review board statement: *The study was approved by Institutional Animal Care and Use Committee of Sun Yat-sen University*

(approval No. SYSU-IACUC-2019-B034) on February 28, 2019.
Copyright license agreement: *The Copyright License Agreement has been signed by all authors before publication.*
Data sharing statement: *Datasets analyzed during the current study are available from the corresponding author on reasonable request.*
Plagiarism check: *Checked twice by iThenticate.*
Peer review: *Externally peer reviewed.*

Open peer reviewer: *Ashley L. Kalinski, University of Michigan, USA.*
Additional files:
Additional Table 1: *Primary and secondary antibodies.*
Additional Figure 1: *ECM proteins in the scaffolds are observed under a fluorescent microscope.*
Additional file 1: *Open peer review report 1.*
Additional file 2: *Original data of this experiment.*

References

Bartholomew M (1988) Reflections of a hospice nurse. Fla Nurse 36:17.
Bedir T, Ulag S, Ustundag CB, Gunduz O (2020) 3D bioprinting applications in neural tissue engineering for spinal cord injury repair. Mater Sci Eng C Mater Biol Appl 110:110741.
Biernaskie J, Sparling JS, Liu J, Shannon CP, Plemel JR, Xie Y, Miller FD, Tetzlaff W (2007) Skin-derived precursors generate myelinating Schwann cells that promote remyelination and functional recovery after contusion spinal cord injury. J Neurosci 27:9545-9559.
Bozkurt G, Mothe AJ, Zahir T, Kim H, Shoichet MS, Tator CH (2010) Chitosan channels containing spinal cord-derived stem/progenitor cells for repair of subacute spinal cord injury in the rat. Neurosurgery 67:1733-1744.
Buckenmeyer MJ, Meder TJ, Prest TA, Brown BN (2020) Decellularization techniques and their applications for the repair and regeneration of the nervous system. Methods 171:41-61.
Cao Z, Yao S, Xiong Y, Zhang Z, Yang Y, He F, Zhao H, Guo Y, Wang G, Xie S, Guo H, Wang X (2020) Directional axonal regrowth induced by an aligned fibrin nanofiber hydrogel contributes to improved motor function recovery in canine L2 spinal cord injury. J Mater Sci Mater Med 31:40.
Cerqueira SR, Lee YS, Cornelison RC, Mertz MW, Wachs RA, Schmidt CE, Bunge MB (2018) Decellularized peripheral nerve supports Schwann cell transplants and axon growth following spinal cord injury. Biomaterials 177:176-185.
Cheng R, Liu L, Xiang Y, Lu Y, Deng L, Zhang H, Santos HA, Cui W (2020) Advanced liposome-loaded scaffolds for therapeutic and tissue engineering applications. Biomaterials 232:119706.
David S, Aguayo AJ (1981) Axonal elongation into peripheral nervous system "bridges" after central nervous system injury in adult rats. Science 214:931-933.
Deng LX, Liu NK, Wen RN, Yang SN, Wen X, Xu XM (2021) Laminin-coated multifilament entubulation, combined with Schwann cells and glial cell line-derived neurotrophic factor, promotes unidirectional axonal regeneration in a rat model of thoracic spinal cord hemisection. Neural Regen Res 16:186-191.
Ding Y, Zhang RY, He B, Liu Z, Zhang K, Ruan JW, Ling EA, Wu JL, Zeng YS (2015) Combination of electroacupuncture and grafted mesenchymal stem cells overexpressing TrkC improves remyelination and function in demyelinated spinal cord of rats. Sci Rep 5:9133.
Elliott Donaghue I, Tator CH, Shoichet MS (2015) Sustained delivery of bioactive neurotrophin-3 to the injured spinal cord. Biomater Sci 3:65-72.
Günther MI, Weidner N, Müller R, Blesch A (2015) Cell-seeded alginate hydrogel scaffolds promote directed linear axonal regeneration in the injured rat spinal cord. Acta Biomater 27:140-150.
Guo JS, Zeng YS, Li HB, Huang WL, Liu RY, Li XB, Ding Y, Wu LZ, Cai DZ (2007) Cotransplant of neural stem cells and NT-3 gene modified Schwann cells promote the recovery of transected spinal cord injury. Spinal Cord 45:15-24.
Hosseinkhani H, Hiraoka Y, Li CH, Chen YR, Yu DS, Hong PD, Ou KL (2013) Engineering three-dimensional collagen-IKVAV matrix to mimic neural microenvironment. ACS Chem Neurosci 4:1229-1235.
Hussein RK, Mencio CP, Katagiri Y, Brake AM, Geller HM (2020) Role of chondroitin sulfation following spinal cord injury. Front Cell Neurosci 14:208.
Johnson PJ, Parker SR, Sakiyama-Elbert SE (2009) Controlled release of neurotrophin-3 from fibrin-based tissue engineering scaffolds enhances neural fiber sprouting following subacute spinal cord injury. Biotechnol Bioeng 104:1207-1214.
Joung D, Truong V, Neitzke CC, Guo SZ, Walsh PJ, Monat JR, Meng F, Park SH, Dutton JR, Parr AM, McAlpine MC (2018) 3D printed stem-cell derived neural progenitors generate spinal cord scaffolds. Adv Funct Mater 28:1801850.
Kaplan B, Merdler U, Szklanny AA, Redenski I, Guo S, Bar-Mucha Z, Michael N, Levenberg S (2020) Rapid prototyping fabrication of soft and oriented polyester scaffolds for axonal guidance. Biomaterials 251:120062.
Lai BQ, Che MT, Du BL, Zeng X, Ma YH, Feng B, Qiu XC, Zhang K, Liu S, Shen HY, Wu JL, Ling EA, Zeng YS (2016) Transplantation of tissue engineering neural network and formation of neuronal relay into the transected rat spinal cord. Biomaterials 109:40-54.
Lai BQ, Che MT, Feng B, Bai YR, Li G, Ma YH, Wang LJ, Huang MY, Wang YQ, Jiang B, Ding Y, Zeng X, Zeng YS (2019) Tissue-engineered neural network graft relays excitatory signal in the completely transected canine spinal cord. Adv Sci (Weinh) 6:1901240.
Li G, Che MT, Zhang K, Qin LN, Zhang YT, Chen RQ, Rong LM, Liu S, Ding Y, Shen HY, Long SM, Wu JL, Ling EA, Zeng YS (2016) Graft of the NT-3 persistent delivery gelatin sponge scaffold promotes axon regeneration, attenuates inflammation, and induces cell migration in rat and canine with spinal cord injury. Biomaterials 83:233-248.
Liu H, Xu X, Tu Y, Chen K, Song L, Zhai J, Chen S, Rong L, Zhou L, Wu W, So KF, Ramakrishna S, He L (2020) Engineering microenvironment for endogenous neural regeneration after spinal cord injury by reassembling extracellular matrix. ACS Appl Mater Interfaces 12:17207-17219.
Liu S, Schackel T, Weidner N, Puttagunta R (2017) Biomaterial-supported cell transplantation treatments for spinal cord injury: Challenges and perspectives. Front Cell Neurosci 11:430.
Lu P, Woodruff G, Wang Y, Graham L, Hunt M, Wu D, Boehle E, Ahmad R, Poplawski G, Brock J, Goldstein LS, Tuszynski MH (2014) Long-distance axonal growth from human induced pluripotent stem cells after spinal cord injury. Neuron 83:789-796.
Mukhamedshina YO, Gracheva OA, Mukhutdinova DM, Chelyshev YA, Rizvanov AA (2019) Mesenchymal stem cells and the neuronal microenvironment in the area of spinal cord injury. Neural Regen Res 14:227-237.
Orr MB, Gensel JC (2018) Spinal cord injury scarring and inflammation: Therapies targeting glial and inflammatory responses. Neurotherapeutics 15:541-553.
Plemel JR, Wee Yong V, Stirling DP (2014) Immune modulatory therapies for spinal cord injury--past, present and future. Exp Neurol 258:91-104.
Qiu XC, Jin H, Zhang RY, Ding Y, Zeng X, Lai BQ, Ling EA, Wu JL, Zeng YS (2015) Donor mesenchymal stem cell-derived neural-like cells transdifferentiate into myelin-forming cells and promote axon regeneration in rat spinal cord transection. Stem Cell Res Ther 6:105.
Rao SN, Pearse DD (2016) Regulating axonal responses to injury: The intersection between signaling pathways involved in axon myelination and the inhibition of axon regeneration. Front Mol Neurosci 9:33.
Smith DR, Dumont CM, Park J, Ciciriello AJ, Guo A, Tatineni R, Cummings BJ, Anderson AJ, Shea LD (2020) Polycistronic delivery of IL-10 and NT-3 promotes oligodendrocyte myelination and functional recovery in a mouse spinal cord injury model. Tissue Eng Part A 26:672-682.
Sparling JS, Bretzner F, Biernaskie J, Assinck P, Jiang Y, Arisato H, Plunet WT, Borisoff J, Liu J, Miller FD, Tetzlaff W (2015) Schwann cells generated from neonatal skin-derived precursors or neonatal peripheral nerve improve functional recovery after acute transplantation into the partially injured cervical spinal cord of the rat. J Neurosci 35:6714-6730.
Stephenson EL, Yong VW (2018) Pro-inflammatory roles of chondroitin sulfate proteoglycans in disorders of the central nervous system. Matrix Biol 71-72:432-442.
Sun JH, Li G, Wu TT, Lin ZJ, Zou JL, Huang LJ, Xu HY, Wang JH, Ma YH, Zeng YS (2020) Decellularization optimizes the inhibitory microenvironment of the optic nerve to support neurite growth. Biomaterials 258:120289.
Tsintou M, Dalamagkas K, Makris N (2020) Taking central nervous system regenerative therapies to the clinic: curing rodents versus nonhuman primates versus humans. Neural Regen Res 15:425-437.
Unal DB, Caliari SR, Lampe KJ (2019) Engineering biomaterial microenvironments to promote myelination in the central nervous system. Brain Res Bull 152:159-174.
Walker CL, Wang X, Bullis C, Liu NK, Lu Q, Fry C, Deng L, Xu XM (2015) Biphasic bisperoxovanadium administration and Schwann cell transplantation for repair after cervical contusive spinal cord injury. Exp Neurol 264:163-172.
Walker MJ, Xu XM (2018) History of glial cell line-derived neurotrophic factor (GDNF) and its use for spinal cord injury repair. Brain Sci 8:109.
Xing H, Ren X, Yin H, Sun C, Jiang T (2019) Construction of a NT-3 sustained-release system cross-linked with an acellular spinal cord scaffold and its effects on differentiation of cultured bone marrow mesenchymal stem cells. Mater Sci Eng C Mater Biol Appl 104:109902.
Xiong Y, Zeng YS, Zeng CG, Du BL, He LM, Quan DP, Zhang W, Wang JM, Wu JL, Li Y, Li J (2009) Synaptic transmission of neural stem cells seeded in 3-dimensional PLGA scaffolds. Biomaterials 30:3711-3722.
Yang L, Conley BM, Cerqueira SR, Pongkulapa T, Wang S, Lee JK, Lee KB (2020) Effective modulation of CNS inhibitory microenvironment using bioinspired hybrid-nanoscaffold-based therapeutic interventions. Adv Mater 32:e2002578.
Zeng X, Zeng YS, Ma YH, Lu LY, Du BL, Zhang W, Li Y, Chan WY (2011) Bone marrow mesenchymal stem cells in a three-dimensional gelatin sponge scaffold attenuate inflammation, promote angiogenesis, and reduce cavity formation in experimental spinal cord injury. Cell Transplant 20:1881-1899.
Zeng YS, Ding Y, Wu LZ, Guo JS, Li HB, Wong WM, Wu WT (2005) Co-transplantation of schwann cells promotes the survival and differentiation of neural stem cells transplanted into the injured spinal cord. Dev Neurosci 27:20-26.
Zhang RP, Wang LJ, He S, Xie J, Li JD (2016) Effects of magnetically guided, SPIO-labeled, and neurotrophin-3 gene-modified bone mesenchymal stem cells in a rat model of spinal cord injury. Stem Cells Int 2016:2018474.
Zhao J, Sun W, Cho HM, Ouyang H, Li W, Lin Y, Do J, Zhang L, Ding S, Liu Y, Lu P, Zhang K (2013) Integration and long distance axonal regeneration in the central nervous system from transplanted primitive neural stem cells. J Biol Chem 288:164-168.

P-Reviewer: Kalinski AL; C-Editor: Zhao M; S-Editors: Yu J, Li CH; L-Editors: Patel B, Yu J, Song LP; T-Editor: Jia Y

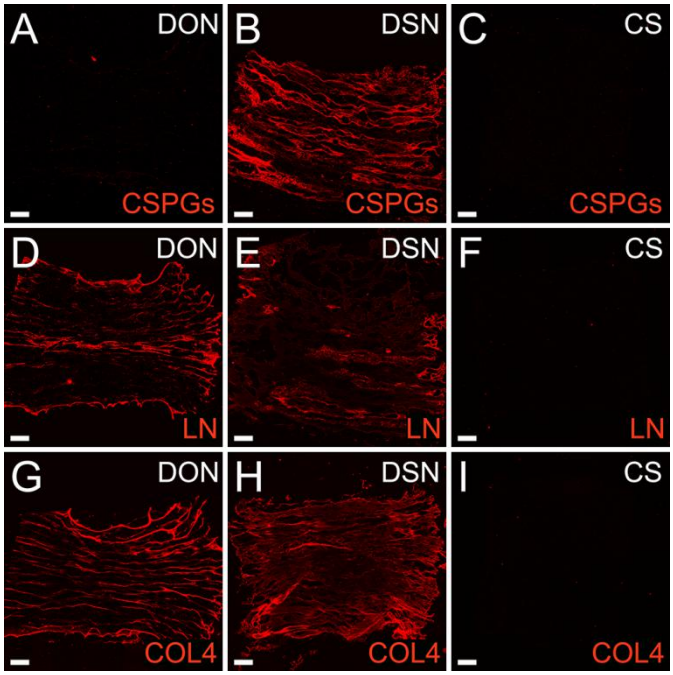

Additional Figure 1 ECM proteins in the scaffolds are observed under a fluorescent microscope.
(A-I) Distribution of CSPGs (A-C), LN (D-F) and COL4 (G-I) in the DON, DSN and CS scaffolds. Scale bars: 400 μm. COL4: Collagen IV; CS: collagen sponge; CSPGs: chondroitin sulfate proteoglycans; DON: decellularized optic nerve; DSN: decellularized sciatic nerve; ECM: extracellular matrix; LN: laminin.

Additional Table 1 Primary and secondary antibodies

Antibodies	Dilution	Source
Mouse anti-CSPGs	1:200	Merck, Hunterdon, NJ, USA
Rabbit anti-LN	1:200	Abcam, Cambridge, UK
Rabbit anti-COL4	1:600	Invitrogen, Carlsbad, CA, USA
Rabbit anti-Nestin	1:200	Sigma-Aldrich, St. Louis, MO, USA
Mouse anti-NF	1:200	BioLegend, San diego, CA, USA
Chicken anti-MBP	1:500	Abcam, Cambridge, UK
Rabbit anti-S100	1:200	Boster, Wuhan, China
Rabbit anti-NT-3	1:200	Sigma, St. Louis, MO, USA
Rabbit anti-IBA-1	1:200	Abcam, Cambridge, UK
Alexa Fluor 647 goat anti-chicken antibody	1:500	Cell Signaling Technology, Boston, MA, USA
Alexa Fluor 555 goat anti-mouse antibody	1:500	Cell Signaling Technology, Boston, MA, USA
Alexa Fluor 555 goat anti-rabbit antibody	1:500	Cell Signaling Technology, Boston, MA, USA

COL4: Collagen IV; CSPGs: chondroitin sulfate proteoglycans; IBA-1: ionized calcium binding adaptor molecule 1; LN: laminin; MBP: myelin basic protein; NF: neurofilament; NT-3: neurotrophin-3.

Mean intensity

			DON					DSN					CS		
CSPGs	3.971	4.239	3.987	3.796	4.196	27.465	28.55	29.978	27.953	27.178	3.217	3.502	3.622	3.839	3.764
LN	14.014	12.885	12.669	12.256	13.747	9.369	13.2467	11.239	10.469	9.261	3.646	3.902	3.859	3.705	3.976
COL4	30.395	28.044	31.58	31.045	26.629	17.635	23.379	24.985	23.783	18.928	3.4655	3.613	3.553	3.539	3.474

NSC viability

DON	DSN	CS
1.053	0.823	0.981
0.985	0.836	0.974
0.941	0.848	0.942
1.159	0.916	0.968
0.998	0.926	0.993
1.096	0.822	0.99
0.977	0.843	1.025
1.104	0.892	1.044
1.042	0.857	1.119

Length of NF positive neurites

DON	DSN	CS
846.46	531.35	307.25
905.54	428.46	346.58
790.75	502.16	385.32
839.61	455.95	338.86
868.37	492.34	395.14

Area of NF positive neurites

DON	DSN	CS
162.1	72.33	50.758
135.22	85.09	39.34
126.46	100.23	54.02
144.09	80.91	65.79
130.73	93.57	60.45

% of directional neurites

DON	DSN	CS
80.9	74.6	25.9
87.2	76.2	33.4
85.8	80.5	28.8
78.2	78.4	36.2

82.5	84.3	29.8

SCs

DON	DSN	CS
151	88	26
136	75	35
129	90	41
147	82	39
142	92	32

Area of NF positive axons

DON	CS
28.5	14.3
24.6	19.4
19.4	9.1
20.7	13
25.9	16.8

Area of MBP positive cells

DON	CS
35.1	23.5
28.5	24.6
24.6	18.1
32.4	13
22	23.3

% of directional axons

DON	CS
80	42
82	28
72	24
66	38
68	54

Myelin sheaths

DON	CS
27	13

28	14
35	20
37	12
31	16
34	12
36	10
29	15
33	18

IBA-1 positive cells

			DON					CS		
Rostral	102	89	95	79	105	203	220	229	215	219
Injury/graft	61	54	69	47	53	200	219	223	215	211
Caudal	112	89	95	99	105	213	220	229	235	248

CSPGs positive area

			DON				CS			
Rostral	25.3	33.2	39.8	29	45.7	72.9	76.4	85.7	68.8	74.8
Injury/graft	13.6	11.9	18	22.6	14.6	63.6	68.3	75.6	58.4	71.9
Caudal	28.6	26	25.8	27.6	46.5	81.1	77.5	71.5	65.3	71.2